Methods

Host–parasite system

Potamopyrgus antipodarum serves as the first intermediate host to at least a dozen species of digenetic trematodes. One of these trematode species, *Microphallus* sp., produces encysted larvae (metacercariae) in the snail in 3–4 months under laboratory conditions. The cysts 'hatch' after ingestion by the final host (waterfowl and wading birds), and the resulting hermaphroditic worms produce cross-fertilized eggs within several days; these eggs then pass into the environment. We have found that mice can serve as the final host in laboratory experiments. Snails become exposed to infection after the ingestion of these eggs. An infection resulting from a single egg results in the production of hundreds (or more) asexual larvae within the same snail, thereby sterilizing the host. These larvae then encyst in the snail, but they can be easily removed by dissection.

Experimental infections

Infections of *Potamopyrgus* were carried out in the laboratory (Edward Percival Field Station in Kaikoura, New Zealand) in January 1997 using mice as the final host. Parasite lines were created within 12 laboratory mice by feeding each mouse the metacercarial cysts from 24 infected snails. Four Lake Poerua parasite lines were created using cysts dissected from 24 infected snails collected from the Lake Poerua shoreline; similarly, 4 Lake Ianthe lines were created using cysts from 24 infected snails collected from the Lake Ianthe shoreline. In addition, 4 'mixed' parasite lines were created by combining cysts from 12 infected Lake Poerua snails with 12 infected Lake Ianthe snails. Assuming random mating, 50% of the parasite eggs would be F_1 hybrid genotypes, 25% would be from Poerua × Poerua crosses, and 25% would be from Ianthe × Ianthe crosses. Of the four parasite lines from each parasite source (pure Poerua, pure Ianthe and mixed), two lines were used to infect Lake Poerua snails, and two lines were used to infect Lake Ianthe snails. Parasite eggs were obtained by repeatedly washing the mouse faecal pellets with water. Eggs were collected between two and six days after the mice ingested the cysts.

For each parasite source, we set up 4 replicate containers with 150 snails from the Lake Poerua shoreline and 4 replicate containers with 150 snails from the Lake Ianthe shoreline. Parasite eggs were added to these containers. Snails were kept in the containers with the parasite eggs for 24 days, with water changed twice each day. The snails were then transported to Indiana University where they were held in 4 litres of water. The water was changed regularly and the snails were fed on *Spirulina*. Ninety days after exposure to parasite eggs, we dissected 75 snails from each replicate, and recorded their infection status and the developmental stage of the parasite (early germinal cells lead to blastocercariae, which lead to metacercariae). These stages appear sequentially over a period of about 70–100 days. We limited our analysis to those snails that were infected in the laboratory (that is, early stage infections). We preserved snail tissue samples (head and foot) of Lake Poerua snails for electrophoretic analysis. We used the resulting five-locus allozyme genotypes to identify clonal lineages[15,16]. We further classified these snails as either 1 of 4 recently common clones (clones 12, 19, 22, 63), which accounted for 50% of the sample, or as rare clones, which contained individuals from 89 different clonal lineages.

Infection rate analysis

For results shown in Fig. 1, statistical analysis was conducted using SPSS[18] on untransformed data, where the dependent variable was mean prevalence of infection for the four replicates within a treatment combination (sympatric versus non-sympatric). The homogeneity-of-variance assumption of the analysis was not violated (Bartlett's Box test: $F_{1,23} = 0.145$; $P = 0.706$).

For results shown in Fig. 2, we used a hierarchical log-linear analysis, with replicate, clone identity and infected as factors. For each of the parasite sources, we examined clone-by-infected interaction terms for common clones and rare clones as groups. Significant interactions would indicate that *Microphallus* sources differentially infected rare versus common clones. We also examined clone-by-infected terms for the four common clones individually to see whether they were differentially infected. We report likelihood ratio χ^2 statistics from a backward model selection routine in SPSS[18]. Main and interaction effects involving replicates were non-significant except for the replicate-by-infected term for the mixed source.

Received 6 December 1999; accepted 10 April 2000.

1. Jaenike, J. An hypothesis to account for the maintenance of sex within populations. *Evol. Theor.* **3,**191–194 (1978).
2. Bremermann, H. J. Sex and polymorphism as strategies in host–pathogen interactions. *J. Theor. Biol.* **87,** 671–702 (1980).
3. Hamilton, W. D. Sex versus non-sex versus parasite. *Oikos* **35,** 282–290 (1980).
4. Seger, J. & Hamilton, W. D. in *The Evolution of Sex* (eds Michod, R. E. & Levin, B. R.) 176–193 (Sinauer and Associates, Sunderland, 1988).
5. Nee, S. Antagonistic coevolution and the evolution of genotype randomization. *J. Theor. Biol.* **140,** 499–518 (1989).
6. Hamilton, W. D., Axelrod, R. & Tanese, R. Sexual reproduction as an adaptation to resist parasites (A review). *Proc. Natl Acad. Sci. USA* **87,** 3566–3573 (1990).
7. Howard, R. S. & Lively, C. M. Parasitism, mutation accumulation and the maintenance of sex. *Nature* **367,** 554–557 (1994).
8. Peters, A. D. & Lively, C. M. The Red Queen and fluctuating epistasis: a population genetic analysis of antagonistic coevolution. *Am. Nat.* **154,** 393–405 (1999).
9. Judson, O. P. Preserving genes: a model of the maintenance of genetic variation in a metapopulation under frequency-dependent selection. *Genetic. Res.* **65,** 175–191 (1995).
10. Gandon, S., Capoweiz, Y., Dubois, Y., Michalakis, Y. & Olivieri, I. Local adaptation and gene-for-gene coevolution in a metapopulation model. *Proc. R. Soc. B* **263,** 1003–1009 (1996).
11. Lively, C. M. Migration, virulence, and the geographic mosaic of adaptation by parasites. *Am. Nat.* **153,** S34–S47 (1999).
12. Parker, M. Local population differentiation for compatibility in an annual legume and its host-specific fungal pathogen. *Evolution* **39,** 713–723 (1985).
13. Lively, C. M. Adaptation by a parasitic trematode to local populations of its host. *Evolution* **46,** 1663–1671 (1989).
14. Ebert, D. Virulence and local adaptation of a horizontally transmitted parasite. *Science* **256,** 1084–1086 (1994).
15. Dybdahl, M. D. & Lively, C. M. Diverse, endemic and polyphyletic clones in mixed populations of the freshwater snail *Potamopyrgus antipodarum*. *J. Evol. Biol.* **8,** 385–398 (1995).
16. Dybdahl, M. F. & Lively, C. M. Host–parasite coevolution: evidence for rare advantage and time-lagged selection in a natural population. *Evolution* **52,** 1057–1066 (1998).
17. Dybdahl, M. F. & Lively, C. M. The geography of coevolution: comparative population structures for a snail and its trematode parasite. *Evolution* **50,** 2264–2275 (1996).
18. Norusis, M. J. *SPSS Advanced Statistics User's Guide* (SPSS, Chicago, 1990).

Acknowledgements

We thank L. Delph for helpful comments on the manuscript. This study was supported by the US National Science Foundation.

Correspondence and requests for materials should be addressed to M.F.D. (e-mail: dybdahl@ohiou.edu) or C.M.L. (e-mail: clively@indiana.edu).

Adhesive force of a single gecko foot-hair

Kellar Autumn*, Yiching A. Liang†, S. Tonia Hsieh‡, Wolfgang Zesch§, Wai Pang Chan‡, Thomas W. Kenny†, Ronald Fearing§ & Robert J. Full‡

* *Department of Biology, Lewis and Clark College, Portland, Oregon 97219, USA*
† *Department of Mechanical Engineering, Stanford University, Stanford, California 94305, USA*
‡ *Department of Integrative Biology, University of California at Berkeley, Berkeley, California 94720, USA*
§ *Department of Electrical Engineering and Computer Science, University of California at Berkeley, Berkeley, California 94720, USA*

Geckos are exceptional in their ability to climb rapidly up smooth vertical surfaces[1–3]. Microscopy has shown that a gecko's foot has nearly five hundred thousand keratinous hairs or setae. Each 30–130 μm long seta is only one-tenth the diameter of a human hair and contains hundreds of projections terminating in 0.2–0.5 μm spatula-shaped structures[2,4]. After nearly a century of anatomical description[2,4–6], here we report the first direct measurements of single setal force by using a two-dimensional micro-electro-mechanical systems force sensor[7] and a wire as a force gauge. Measurements revealed that a seta is ten times more effective at adhesion than predicted from maximal estimates on whole animals. Adhesive force values support the hypothesis that individual seta operate by van der Waals forces[8,9]. The gecko's peculiar behaviour of toe uncurling and peeling[2] led us to discover two aspects of setal function which increase their effectiveness. A unique macroscopic orientation and preloading of the seta increased attachment force 600-fold above that of frictional measurements of the material. Suitably orientated setae reduced the forces necessary to peel the toe by simply detaching above a critical angle with the substratum.

The foot of a Tokay gecko (*Gekko gecko*) has about 5,000 setae mm^{-2} (ref. 4) and can produce 10 N of adhesive force with approximately 100 mm^2 of pad area[10] (Fig. 1a–d). Therefore, each seta should produce an average force of 20 μN and an average stress of 0.1 N mm^{-2} (~1 atm). The actual magnitudes could be greater, as it is unlikely that all setae adhere simultaneously. We measured force production by single, isolated seta during attachment using a micromachined, dual-axis, piezoresistive cantilever (Fig. 1e).

To determine how setal force should be measured, we considered

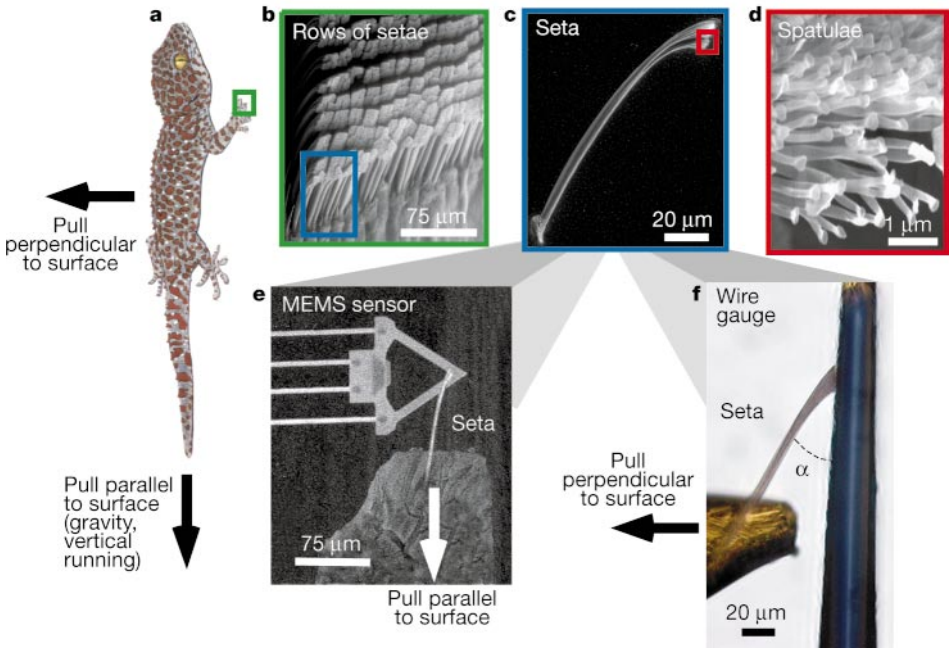

Figure 1 Gecko setae and apparatus for force measurement. **a**, Tokay gecko (*Gekko gecko*) with toe outlined. **b–d**, SEMs of rows of setae from a toe (**b**), a single seta (**c**) and, the finest terminal branches of a seta, called spatulae (**d**). **e**, Single seta attached to a micro-electromechanical system (MEMS) cantilever[7] capable of measuring force production during attachment parallel and perpendicular to the surface. **f**, Single seta attached to an aluminum bonding wire capable of measuring force production during detachment perpendicular to the surface. Angle between setal stalk and wire represented by α.

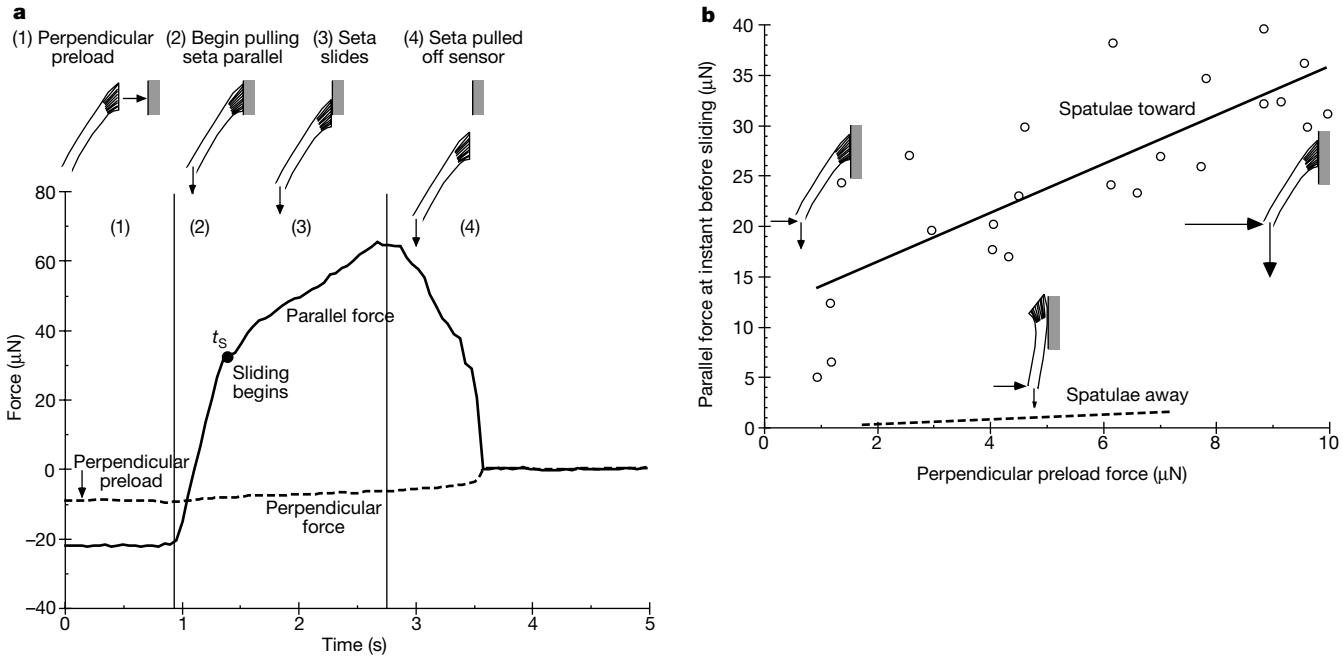

Figure 2 Force of single seta pulled parallel to the surface with a known perpendicular preload. **a**, Submaximal force (solid line) as a function of time. Perpendicular preload is designated by the dashed line. t_s represents the time when the seta began to slide off the sensor. The initial perpendicular force need not be maintained during the subsequent pull. Diagrams show the stages of setal movement corresponding to the force record. Arrows indicate the direction of applied force to the seta. Vertical arrow indicates a parallel force, and a horizontal arrow indicates a perpendicular force. Parallel force was zero prior to force application, and both parallel and perpendicular forces return to zero following force application. **b**, Setal force parallel to the surface during attachment as a function of perpendicular preload force. Setal force was taken to be the adhesive force at the time just prior to sliding (t_s). The solid line represents a seta with spatulae projecting toward the surface. Results from a single seta are shown (parallel force $= 2.8 \times$ perpendicular preload $+ 10.1$; $r^2 = 0.74$; $n = 41$; $F = 113$; d.f. $= 1, 39$; $P < 0.0001$), but did not differ significantly in slope (analysis of covariance, variance ratio $F = 2.1$; degrees of freedom d.f. $= 4, 57$; $P = 0.10$) or intercept ($F = 0.052$; d.f. $= 4, 57$; $P = 0.99$) among five setae. The dashed line represents the setal force with spatulae projecting away from the surface (parallel force $= 0.25 \times$ perpendicular preload $- 0.09$; $r^2 = 0.64$; $F = 13$; d.f. $= 1, 9$; $P = 0.007$). The force produced by the inactive, non-spatular region increased with normal or perpendicular force, typical of materials with a coefficient of friction equal to 0.25. The perpendicular preloading force that could be applied attained a maximum (near 15 μN), because greater forces resulted in setal buckling.

the gecko's unusually complex behaviour of toe uncurling during attachment, which is much like blowing up an inflating party favour, and toe peeling during detachment, analogous to removing a piece of tape from a surface. The exquisite control of the toe allowed us to discover aspects of setal function by indicating that orientation and loading could be crucial to setal force capacity. Setal force did, in fact, depend on three-dimensional orientation (spatulae pointing towards or away from the surface) and the extent to which the seta was preloaded (pushed into and pulled along the surface) during the initial contact. Contacting the surface with the seta in a direction other than with spatulae projecting toward the surface resulted in forces of less than 0.3 μN when the seta was pulled away perpendicular to the surface. By contrast, when the active spatular region was projecting toward the surface, force increased enormously. After an initial push toward the surface, a 'perpendicular preload', the seta was pulled parallel to the surface. Setal adhesive force parallel to the surface increased until the seta began to slide off the edge of the sensor (at time t_s, Fig. 2a). Setal force parallel to the surface increased linearly with the perpendicular preloading force and was substantially greater than the force produced by the inactive, non-spatular region at all preloads (Fig. 2b). Experiments in which setae were pulled away from the surface of a wire (Fig. 1f) demonstrated that perpendicular preloading alone is insufficient for effective setal attachment. Setae that were first pushed into the surface and then pulled parallel to it developed over ten times the force (13.6 ± 2.6 μN; $n = 17$) upon being pulled away from the surface than those having only a perpendicular preload (0.6 ± 0.7 μN; $n = 17$). The largest parallel forces were observed only if the seta was allowed to slide approximately 5 μm along the sensor's surface, a distance imperceptible at the level of the foot (Fig. 3). The maximum adhesive force of single seta averaged 194 ± 25 μN ($n = 28$), nearly tenfold greater than predicted from whole animal estimates. Our single-seta force measurements indicate that if all setae were simultaneously and maximally attached, a single foot of a gecko could produce 100 N of adhesive force (~10 atm). The results of preloading on setal force production support the hypothesis that a small perpendicular preloading force in concert with a rearward displacement or parallel preload may be necessary to engage adhesion[4]. Because the tips of the setae are directed rearwards away from the toenail, preloading may increase the number of spatulae contacting the surface[11].

The orientation of the setae was also important in detachment. We found that setae detached at a similar angle (30.6 ± 1.8°; $n = 17$) when pulled away from the wire sensor's surface. To check for the presence of a critical angle of detachment, we controlled perpendicular force and progressively increased the setal angle (α; Fig. 1f) until detachment. Setal angle at detachment changed by only 15% over a range of perpendicular forces (Fig. 4). This observation is consistent with an adhesive model where sliding stops when pulling at greater than the critical setal angle, and hence stress can increase at a boundary, causing fracture of the contact. Change in the orientation of the setae and perhaps even the geometry of the spatulae may help detachment. Geckos peel the tips of their toes away from a smooth surface during running[2]. This toe peeling may have two effects. First, as we discovered here, it may put an individual seta in an orientation or at a critical angle that aids in its release. Second, toe peeling concentrates the detachment force on only a small subset of all attached setae at any instant.

Our direct setal force measurements reject two of the proposed mechanisms of adhesion, suction[12,13] and friction[6,14], and provide indirect support for the most favoured hypothesis, intermolecular forces[8,9]. Our measurements of greater than one atmosphere of adhesion pressure indicate that suction is not involved and support previous measurements carried out in a vacuum[5]. The present data do not support a friction mechanism[6,14] because the coefficient of friction of the setal keratin on silicon is low ($\mu = 0.25$; Fig. 2b; dashed line). Microinterlocking[14] could function as a secondary mechanism, but the cantilever's surface was smooth (surface roughness less than or equal to 2.5 nm) and the ability of geckos to adhere to polished glass shows that irregularities on the scale of the spatulae are not necessary for adhesion[1]. Previous experiments using X-ray bombardment[5] have eliminated electrostatic attraction[15] as a mechanism necessary for setal adhesion, because the setae can still adhere in ionized air. Adhesion by glue is an unlikely mechanism, as skin glands are not present on the feet of lizards[5,15,16]. However, the role of adsorbed water requires further study[11].

Our direct setal force measurements are consistent with the hypothesis that adhesion in geckos is the result of intermolecular forces[8,9]. Earlier experimental support for the van der Waals hypothesis[4,9] comes from the observation that adhesive force of a whole gecko increases with increasing surface energy of the substrate[8,9]. The simple models available can only give the most approximate estimates of setal force production. If we assume that the tip of a spatula is a curved segment of a sphere (radius,

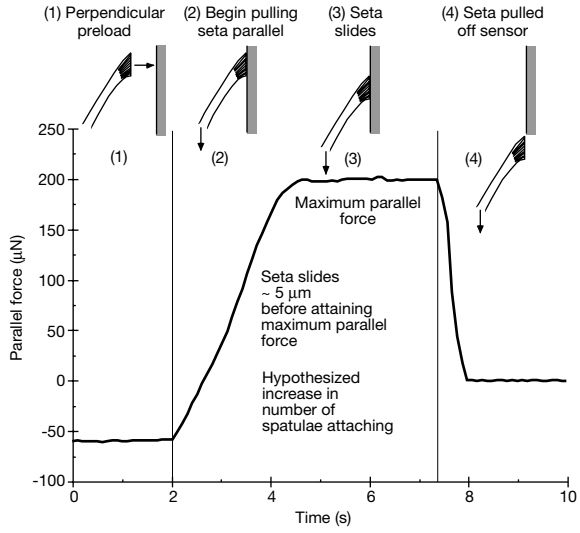

Figure 3 Maximal force after a maximum preload (~15 μN) of a single seta parallel to the surface as a function of time. Diagrams show the stages of setal movement corresponding to the force record from the MEMS cantilever (Fig. 1e). Arrows indicate the direction of force applied to the seta. Vertical arrow indicates a parallel force; horizontal arrow indicates a perpendicular force. The maximum force following the small rearward displacement (~5 μm) was ten times that predicted from whole animal estimates (see text). The large increase in force during the rearward displacement may be caused by an increase in the number of spatulae contacting the surface.

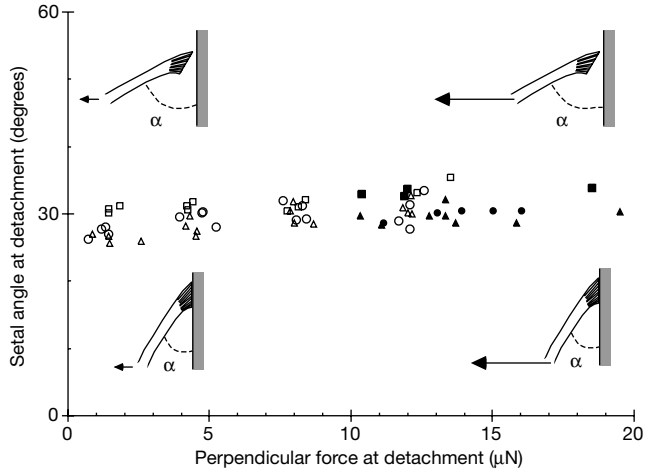

Figure 4 Setal angle (α) with the surface at detachment as a function of perpendicular force. Filled symbols represent seta pulled away from the surface until release. Open symbols represent seta held at a constant force as angle is increased. Each symbol shape represents a different seta. Data collected with wire gauge (Fig. 1f). Perpendicular force had a weak but significant effect on angle at detachment ($\alpha = 0.22 \times$ perpendicular force $+ 28.2$; $r^2 = 0.25$; $F = 20$; d.f. $= 1, 59$; $P < 0.0001$).

$R = 2\,\mu$m) and is separated by a small distance from a large, flat surface where van der Waals forces become significant (atomic gap distance, $D \approx 0.3$ nm), then setal force $= AR/6D^2$ where A is the material-dependent Hamaker constant taken to be 10^{-19} J (ref. 17). This estimate puts the van der Waals force for a spatula to be about 0.4 μN. As the number of spatulae per seta varies from 100 to 1,000, setal force estimates range from 40 to 400 μN, a range within which our direct measurements fall. The uncertainty in this estimate points to the need for future data collection on spatular morphology, orientation, spacing and material properties. van der Waals forces are extremely weak at greater than atomic distance gaps, and require intimate contact between the adhesive and the surface. Polymeric adhesives such as tape are soft, and are able to deform sufficiently for intimate contact over a relatively large surface area[18,19]. The feet of *G. gecko* contain approximately one billion spatulae that could provide a sufficiently large surface area in close contact with the substrate[4] for adhesion to be the result of van der Waals forces. Although manufacturing small, closely packed arrays mimicking setae are beyond the limits of human technology, the natural technology of gecko foot-hairs can provide biological inspiration for future design of a remarkably effective adhesive. □

Methods

Preparation of single seta

We carefully peeled the cuticular layer of a single row of lamellae off the toe of a restrained, live, non-moulting gecko. With a finely etched tungsten pin, we scraped the cuticular surface to break off individual setae at the base of the stalk. The isolated seta was then glued to the end of a #2 insect pin with 5-min epoxy (TTWDevcon, Danvars, Massachusetts). The pin had a tip diameter of approximately 15 μm. To prevent the epoxy from creeping up the stalk of the seta, which might change the mechanical property of the specimen, we pre-cured the epoxy for about 1 min before applying it to the specimen. All setae were orientated so that the active surface was roughly perpendicular to the axis of the pin. All preparations were completed under a compound microscope.

Force estimation of a single seta during a parallel pull

To measure force parallel and perpendicular to the surface, we used a micromachined, dual-axis piezoresistive cantilever[7] fabricated on a single-crystalline silicon wafer (Fig. 1e). It had two independent force sensors, each with one predominant direction of compliance. The perpendicular force sensor consisted of a thin triangular probe. The parallel force sensor was composed of four long slender ribs. A special 45° oblique ion implantation allowed piezoresistive and conductive regions to be implanted on both the parallel and perpendicular surfaces simultaneously. Forces applied to the tip of the sensor were resolved into these two orthogonal directions (parallel and perpendicular), and were measured by the changes in resistance of the piezoresistors. The minimum detectable force for these cantilevers, calculated from the noise spectra, is ~5 nN in a 10 kHz bandwidth. Maximum force measurements possible exceed 300 μN. The spring constant of the sensor was calibrated using a commercial force calibration cantilever (ThermoMicroscopes). The displacement sensitivity was obtained by measuring the resistance change of the piezoresistors while deflecting the cantilever by a known distance. As this device was originally designed for atomic force microscope data storage applications, each of these cantilevers had a sharp tip near the vertex of its triangular probe. For the gecko setae adhesion measurement, the back-side of this device was used to provide a smooth surface for setal adhesion.

Each seta was brought in contact with the sensor by applying a small preload perpendicular to the surface to increase contact and induce adhesion. To determine the effect of preload force on submaximal parallel force, we varied preload force when setae were attached to the tip of the sensor (Fig. 2b). To measure maximal parallel force, we used the base of the triangular probe. Using the base increased the area of contact, but did not allow for simultaneous measurement of preload forces. Sensor signals were taken while the seta was being pulled parallel to the surface by a piezoelectric manipulator at a rate of ~5 μm sec^{-1}. Sensor signals were amplified and filtered through a 300-Hz low-pass filter, and then digitized at 100 Hz using a 16-bit data acquisition card (National Instruments). The collected data (in volts) were converted to deflections of the sensor through the displacement sensitivity, and multiplied by the spring constant to obtain force values.

Force estimation of a single seta during a perpendicular pull

Breaking or detachment force was defined as the maximal force a seta could exert perpendicular to a surface immediately before it released. We determined this value for individual seta by measuring the amount it could displace a force gauge made from a 4.7 mm aluminum bonding wire with 25 μm nominal diameter (American Fine Wire Corp., Selman, Alabama; Fig. 1f). To maximize contact area of the active surface of the seta to the wire, we flattened a 50 × 100 μm section at the wire's distal tip. The proximal end of the wire was fixed with epoxy onto a brass stub. We pressed the active surface of the seta against the flattened wire, producing a known perpendicular preload (1.6 ± 0.25 μN SD). We applied a perpendicular detachment force to the seta using two different methods. (1) We pulled the seta perpendicular to the wire. (2) We displaced the insect pin 19.7 ± 3.45 μm along the wire to produce an additional parallel preload on the seta before pulling perpendicular to the wire. We then applied perpendicular detachment forces ranging from 0.5 to 20 μN and increased the angle of the seta with respect to the wire (α) until detachment occurred.

In all trials, detachment force was calculated from the maximum displacement of the wire pulled by the seta. All sequences were recorded with a video camera (Sony CCD) and digitized to a computer using a video editing system (Media 100 Inc., Marlboro, Massachusetts). The initial position of the wire, the angle of the seta with respect to the wire (α) and the position of the wire at the point of separation were recorded and analysed using image analysis software (NIH-Image). The amount of deflection in the force gauge was converted to adhesion force after we calibrated the force gauge against standard weights.

Received 31 January; accepted 27 March 2000.

1. Maderson, P. F. A. Keratinized epidermal derivatives as an aid to climbing in gekkonid lizards. *Nature* **203,** 780–781 (1964).
2. Russell, A. P. A contribution to the functional morphology of the foot of the tokay, *Gekko gecko* (Reptilia, Gekkonidae). *J. Zool. Lond.* **176,** 437–476 (1975).
3. Cartmill, M. in *Functional Vertebrate Morphology* (eds Hildebrandt, M., Bramble, D. M., Liem, K. F. & Wake, D. B.) 73–88 (Harvard Univ. Press, Cambridge, Massachusetts, 1985).
4. Ruibal, R. & Ernst, V. The structure of the digital setae of lizards. *J. Morphol.* **117,** 271–294 (1965).
5. Dellit, W.-D. Zur anatomie und physiologie der Geckozehe. *Jena Z. Naturw.* **68,** 613–656 (1934).
6. Hora, S. L. The adhesive apparatus on the toes of certain geckos and tree frogs. *J. Proc. Asiatic Society of Bengal.* **9,** 137–145 (1923).
7. Chui, B. W., Kenny, T. W., Mamin, H. J., Terris, B. D. & Rugar, D. Independent detection of vertical and lateral forces with a sidewall-implanted dual-axis piezoresistive cantilever. *Appl. Phys. Lett.* **72,** 1388–1390 (1998).
8. Hiller, U. Form und funktion der hautsinnesorgane bei gekkoniden. *Form. Funct.* **4,** 240–253 (1971).
9. Hiller, U. Untersuchungen zum Feinbau und zur Funktion der Haftborsten von Reptilian. *Z. Morphol. Tiere* **62,** 307–362 (1969).
10. Irschick, D. J. *et al.* A comparative analysis of clinging ability among pad-bearing lizards. *Biol. J. Linnaen Soc.* **59,** 21–35 (1996).
11. Stork, N. E. Experimental analysis of adhesion of *Chrysolina polita* (Chrysomelidae: Coleoptera) on a variety of surfaces. *J. Exp. Biol.* **88,** 91–107 (1980).
12. Gadow, H. *The Cambridge Natural History Vol. 8 Amphibia and Reptiles* (McMillan, London, 1901).
13. Gennaro, J. G. J. The gecko grip. *Natural History* **78,** 36–43 (1969).
14. Mahendra, B. C. Contributions to the bionomics, anatomy, reproduction and development of the Indian house gecko *Hemidactylus flaviviridis* Ruppell. Part II. The problem of locomotion. *Proc. Indian Acad. Sci.* **3,** 288–306 (1941).
15. Schmidt, H. R. Zur Anatomie und Physiologie der Geckopfote. *Jena Z. Naturw.* **39,** 551 (1904).
16. Bellairs, A. *The life of reptiles* (Universe, New York, 1970).
17. Israelachvili, J. *Intermolecular & Surface Forces* (Academic, New York, 1992).
18. Kinloch, A. J. *Adhesion and adhesives: science and technology* (Chapman and Hall, New York, 1987).
19. Gay, C. & Leibler, L. Theory of tackiness. *Phys. Rev. Lett.* **82,** 936–939 (1999).

Acknowledgements

Supported by IS Robotics, a DARPA/ONR grant to R.J.F., an ONR MURI, NSF Graduate Research Fellowship, and NSF career and XYZ on a Chip awards to T.W.K. Fabrication of the MEMS devices used the Stanford Nanofabrication Facility. We thank S. Block,

K. Meijer, D. Dudek, A. Ahn, T. Kubow and J. Hearst for comments on earlier drafts, E. Florance for electron microscopy, the University of California Museum of Paleontology electron microscope laboratory and the Scientific Visualization Center at Berkeley.

Correspondence and requests for materials should be addressed to R.J.F. (e-mail: rjfull@socrates.berkeley.edu).

Neural synchrony correlates with surface segregation rules

Miguel Castelo-Branco, Rainer Goebel, Sergio Neuenschwander & Wolf Singer

Max-Planck-Institut für Hirnforschung, Deutschordenstraße 46, 60528 - Frankfurt am Main, Germany

To analyse an image, the visual system must decompose the scene into its relevant parts. Identifying distinct surfaces is a basic operation in such analysis, and is believed to precede object recognition[1,2]. Two superimposed gratings moving in different directions (plaid stimuli) may be perceived either as two surfaces, one being transparent and sliding on top of the other (component motion) or as a single pattern whose direction of motion is intermediate to the component vectors (pattern motion)[3–6]. The degree of transparency, and hence the perception, can be manipulated by changing only the luminance of the grating intersections[7–12]. Here we show that neurons in two visual cortical areas—A18 and PMLS—synchronize their discharges when responding to contours of the same surface but not when responding to contours belonging to different surfaces. The amplitudes of responses correspond to previously described rate predictions[3,13–16] for component and pattern motion, but, in contrast to synchrony, failed to reflect the transition from component to pattern motion induced by manipulating the degree of transparency. Thus, dynamic changes in synchronization could encode, in a context-dependent way, relations among simultaneous responses to spatially superimposed contours and thereby bias their association with distinct surfaces.

Specialized visual neurons may signal the motion of either the individual gratings of a plaid (component-selective cells) or of the global pattern (pattern-selective cells). For the identification of these cells, responses evoked by single gratings were compared to those evoked by unambiguous plaid patterns moving in an intermediate direction, and the results indicate that both cell types exist[3,13–16]. However, except for a single study in the motion sensitive area (MT)of monkey visual cortex[11], no attempt has been made to investigate changes in response amplitudes associated with gradual modifications of transparency conditions. Therefore, little is known about how well individual cells differentiate between component and pattern motion.

Here, we investigate this question with multi-electrode recordings from neurons located in areas A18 and PMLS (postero-medial bank of the lateral suprasylvian sulcus) of the cat visual cortex. In addition, we use cross-correlation analysis to examine the hypothesis that binding of the moving contours into one coherent pattern or two independently moving gratings is associated with changes in the synchronization of responses.

Neurons synchronize their discharges with a precision in the millisecond range if they are activated by single contours, but they do not synchronize when activated by contours of different objects[17–20]. It has been proposed, therefore, that synchronization serves as a binding mechanism by virtue of selectively raising the saliency of the synchronized discharges and thereby favouring their joint processing at subsequent levels. Accordingly, when exposed to plaid stimuli, cells responding to contours of the same surface should synchronize their responses, and cells activated by contours belonging to different surfaces should not synchronize. Which cells are associated with a particular surface depends on transparency conditions, on the match of the cells' preferred direction of motion with the direction of motion of the plaid components and on the spatial relation (overlap, colinearity) of the receptive fields (RFs). In pattern motion, all cells capable of responding to the respective component motions should synchronize their responses because they are excited by contours of the same surface. In component motion, only those cells that respond to the contours of the same component grating should synchronize. This synchronization

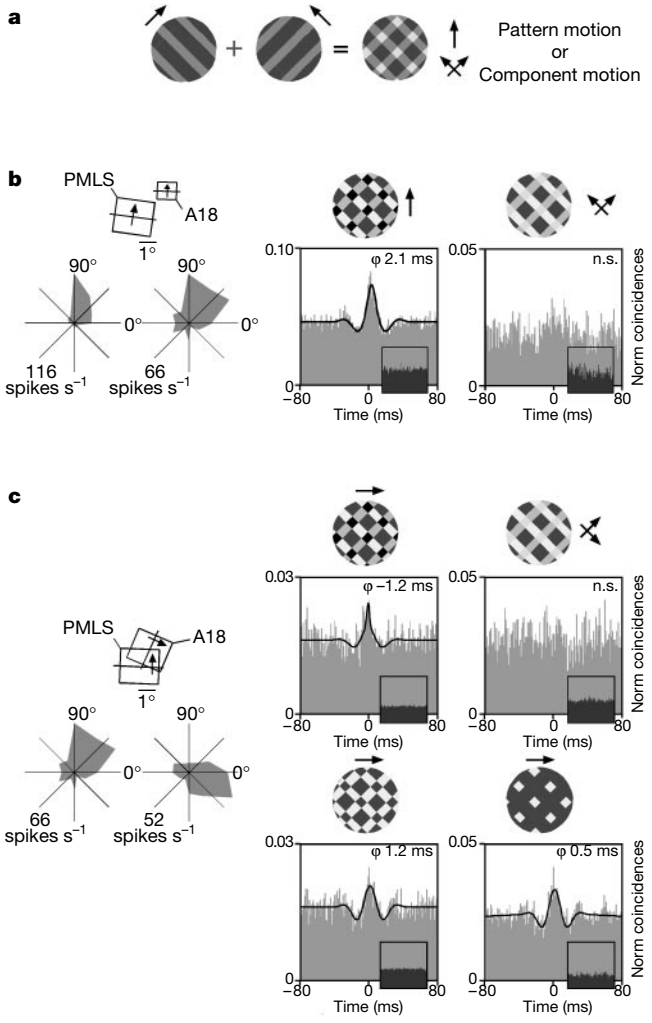

Figure 1 Dependence of synchrony on transparency conditions and receptive field (RF) configuration. **a**, Stimulus configuration. **b**, Synchronization between neurons with non-overlapping RFs and similar directional preferences recorded from A18 and PMLS. Left, RF constellation and tuning curves; right, cross-correlograms for responses to a non-transparent (left) and transparent plaid (right) moving in the cells' preferred direction. Grating luminance was asymmetric to enhance perceptual transparency[3]. Small dark correlograms are shift predictors. **c**, Synchronization between neurons with different direction preferences recorded from A18 (polar and RF plots, left). Top, correlograms of responses evoked by a non-transparent (left) and a transparent (right) plaid moving in a direction intermediate to the cells' preferences. Bottom, correlograms of responses evoked by a non-transparent plaid with reversed contrast conditions (left), and by a surface defined by coherent motion of intersections (right). Scale on polar plots: discharge rate in spikes per second. Scale on correlograms: abscissa, shift interval in ms, bin width 1 ms; ordinate, number of coincidences per trial, normalized. Thick line, fitted gabor function; φ, phase shift. n.s., not significant.